



Individual identification of free hole and electron dynamics in $\text{CuIn}_{1-x}\text{Ga}_x\text{Se}_2$ thin films by simultaneous monitoring of two optical transitions

Makoto Okano, Hideki Hagiya, Takeaki Sakurai, Katsuhiko Akimoto, Hajime Shibata, Shigeru Niki, and Yoshihiko Kanemitsu

Citation: *Applied Physics Letters* **106**, 181903 (2015); doi: 10.1063/1.4919902

View online: <http://dx.doi.org/10.1063/1.4919902>

View Table of Contents: <http://scitation.aip.org/content/aip/journal/apl/106/18?ver=pdfcov>

Published by the AIP Publishing

Articles you may be interested in

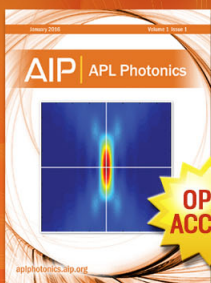
Charge-carrier dynamics in polycrystalline thin-film $\text{CuIn}_{1-x}\text{Ga}_x\text{Se}_2$ photovoltaic devices after pulsed laser excitation: Interface and space-charge region analysis
J. Appl. Phys. **117**, 185102 (2015); 10.1063/1.4921011

Charge carrier dynamics and recombination in graded band gap $\text{CuIn}_{1-x}\text{Ga}_x\text{Se}_2$ polycrystalline thin-film photovoltaic solar cell absorbers
J. Appl. Phys. **114**, 154505 (2013); 10.1063/1.4825211

Nanostructured light-absorbing crystalline $\text{CuIn}_{(1-x)}\text{Ga}_x\text{Se}_2$ thin films grown through high flux, low energy ion irradiation
J. Appl. Phys. **114**, 153505 (2013); 10.1063/1.4823987

Investigation of deep-level defects in $\text{Cu}(\text{In,Ga})\text{Se}_2$ thin films by two-wavelength excitation photo-capacitance spectroscopy
Appl. Phys. Lett. **103**, 163905 (2013); 10.1063/1.4826144

Effect of Ga content on defect states in $\text{CuIn}_{1-x}\text{Ga}_x\text{Se}_2$ photovoltaic devices
Appl. Phys. Lett. **80**, 4540 (2002); 10.1063/1.1485301



Launching in 2016!
The future of applied photonics research is here

AIP | APL
Photonics

Individual identification of free hole and electron dynamics in $\text{CuIn}_{1-x}\text{Ga}_x\text{Se}_2$ thin films by simultaneous monitoring of two optical transitions

Makoto Okano,¹ Hideki Hagiya,² Takeaki Sakurai,² Katsuhiko Akimoto,² Hajime Shibata,³ Shigeru Niki,³ and Yoshihiko Kanemitsu^{1,4,a)}

¹Institute for Chemical Research, Kyoto University, Uji, Kyoto 611-0011, Japan

²Institute of Applied Physics, University of Tsukuba, Tsukuba, Ibaraki 305-8573, Japan

³National Institute of Advanced Industrial Science and Technology (AIST), Tsukuba, Ibaraki 305-8568, Japan

⁴Japan Science and Technology Agency, CREST, Kyoto University, Uji, Kyoto 611-0011, Japan

(Received 19 January 2015; accepted 27 April 2015; published online 6 May 2015)

The photocarrier dynamics of $\text{CuIn}_{1-x}\text{Ga}_x\text{Se}_2$ (CIGS) thin films were studied using white-light transient absorption (TA) measurements, as an understanding of this behavior is essential for improving the performance of solar cells composed of CIGS thin films. A characteristic double-peak structure due to the splitting of the valance bands in the CIGS was observed in the TA spectra under near-band-gap resonant excitation. From a comparison of the TA decay dynamics monitored at these two peaks, it was found that the slow-decay components of the electron and hole relaxation are on the nanosecond timescale. This finding is clear evidence of the long lifetimes of free photocarriers in polycrystalline CIGS thin films. © 2015 AIP Publishing LLC.

[<http://dx.doi.org/10.1063/1.4919902>]

Owing to their considerable advantages, such as low weight and flexibility, a large variety of thin-film solar cells have been extensively studied.^{1–7} Hence, ternary and multi-ary semiconducting materials have been found to constitute some of the most promising substances for use in efficient thin-film solar cells, because they possess certain advantages such as a large absorption coefficient, cheap and easy fabrication, and optimum band-gap energy.^{1–5} In particular, polycrystalline $\text{CuIn}_{1-x}\text{Ga}_x\text{Se}_2$ (CIGS) exhibits the highest power-conversion efficiency of the various thin-film solar cells and has achieved 21.7% efficiency to date.^{1–3} Because of the high efficiency of polycrystalline CIGS and its unique superiority over its single-crystal counterparts, during the past three decades, numerous experimental and theoretical studies have been conducted to characterize the optical and electronic properties of this material.^{8–12} Indeed, many studies have been conducted on the grain boundaries and defect states of this substance, which play an important role in the optoelectronic conversion processes of polycrystalline CIGS.^{13–18} At present, to further improve the solar-cell performance of polycrystalline CIGS films and to determine the source of their high conversion efficiencies, it is necessary to clarify the free photocarrier dynamics in these materials.

In order to investigate the dynamical behavior of the photocarriers in CIGS, a large number of time-resolved photoluminescence (PL),^{19–25} transient absorption (TA), and transient reflectivity (TR) measurements^{26,27} have been performed. In particular, TA and TR measurement techniques (along with combinations of other methods) are powerful tools for determining free carrier dynamics, which are the main contributors to the photocurrent, in emerging solar cells.^{28–31} To examine the energy relaxation dynamics of photocarriers in complex semiconducting materials such as CIGS films, it is important to monitor the TA decay dynamics over a wide spectral range,

because defects, grain boundaries, composition fluctuations, and electrostatic potential fluctuations affect the near-band-edge electronic structures. This leads to the complicated energy relaxation processes observed in these materials.^{27,31,32} Moreover, broadband monitoring in TA experiments allows for examination of the higher optical transitions, providing essential information on free carrier dynamics.

According to the theoretical calculations,^{8–10} the second-highest valence band (v3) in CIGS exists near the highest valence band (v1), as shown in Fig. 1. Thus, by choosing the optimal pump energy and probing the lowest optical transition between the lowest conduction (c1) and v1 bands (E_{c1-v1} transition), along with the high-energy transition between the c1 and v3 bands (E_{c1-v3} transition), we can individually clarify the relaxation dynamics of the free electrons in the c1 band and the free holes in the v1 band. An improved understanding of the dynamics of each carrier type is of considerable

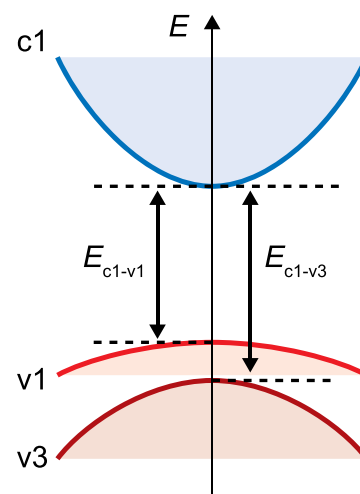


FIG. 1. Schematic band structure of CIGS thin films in the vicinity of the band edge. In the sample used in this work, the E_{c1-v1} and E_{c1-v3} transition energies are approximately 1.21 and 1.45 eV, respectively.

^{a)}kanemitsu@scl.kyoto-u.ac.jp

importance, as this will reveal the optoelectronic properties of the intricate systems involved in the CIGS defects, potential fluctuation, and so on.

In this letter, we report the individual determination of electron and hole lifetimes in CIGS thin films using white-light pump-probe TA spectroscopy. The characteristic absorption structures owing to two E_{c1-v1} and E_{c1-v3} transitions were observed. Even in the case when the excitation energy was equal to the lower energy transition, E_{c1-v1} , we found that the TA signals originated from the same low-energy (E_{c1-v1}) and high-energy (E_{c1-v3}) transitions. By comparing the two types of TA decay dynamics caused by each transition, we determined the lifetimes of the free electrons and holes. The existence of long-lived free carriers was clearly proven, which is an essential factor contributing to the high performance of CIGS-based solar cells.

The CIGS thin-film samples used in this study were deposited directly on soda-lime glass (SLG) substrates of 300-nm thickness using a 3-stage molecular beam epitaxy process.³ The composition of the CIGS samples was Cu-poor ($\text{Cu}/(\text{In} + \text{Ga}) \sim 0.95$), which is required for the high power conversion efficiency of CIGS-based solar cells. Our sample thickness was less than that of the CIGS layer in the practical solar cells used to perform TA measurements with a transmittance configuration. The band-gap depth gradient was negligibly small. To obviate the contamination and oxidation of the CIGS surfaces, a 30-nm-thick CdS layer was deposited on the CIGS layer. TA and PL measurements were then performed using a wavelength-tunable regenerative-amplifier Yb:KGW-based femtosecond laser system with an optical parametric amplifier (OPA) (maximum repetition rate: 200 kHz) as a light source. To generate the white-light probe pulses, femtosecond fundamental pulses of 1028-nm wavelength were focused on a sapphire crystal. For stable generation of the white-light pulse, the repetition rate of the regenerative amplifier was reduced from 200 to 50 kHz, so as to suppress the heating of the sapphire crystal. Part of the regenerative amplifier fundamental pulse was used to generate various pump-pulse energies with the OPA. The PL spectra were measured using a liquid-nitrogen-cooled InGaAs array detector with a 30-cm monochromator. For the PL measurements, the excitation photon energy was set to 1.75 eV to eliminate the PL from the SLG substrates. All measurements were conducted at room temperature.

Figure 2(a) shows the absorption spectrum of the CIGS thin films ranging from 1.0 to 2.0 eV. Two gentle-step structures can be observed at approximately 1.20 and 1.45 eV. To clearly understand the observed absorption structures, we calculated the first-order derivative of the absorption spectrum, as shown in Fig. 2(b). In this figure, two peaks can be observed at approximately 1.21 and 1.45 eV, which are attributed to the onset of the absorption due to the allowed optical transitions from the v1 and v3 bands to the c1 band (the E_{c1-v1} and E_{c1-v3} transitions in Fig. 1), respectively, based on the first-principle calculation.^{8–10} The observed E_{c1-v1} corresponds to the composition of $\text{Ga } x \sim 0.38$.³³

The assignment of the band-to-band transition energies to these peaks is supported by the excitation-fluence dependence of the PL spectra of the CIGS thin films shown in Fig. 2(c). A single PL peak is observed at approximately the

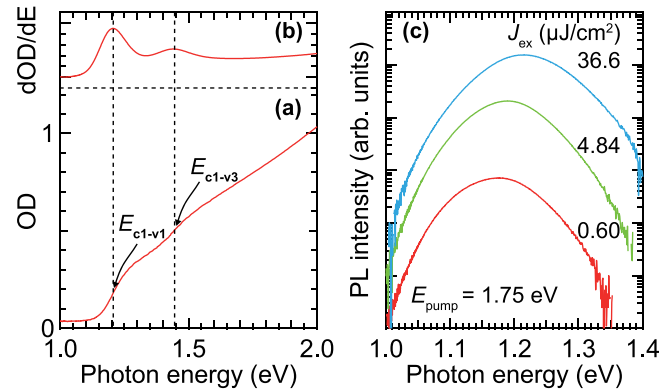


FIG. 2. (a) Absorption spectrum and (b) first-order derivative of the absorption spectrum of CIGS thin films. (c) Dependence of steady-state PL spectra of CIGS thin films on the excitation fluence (J_{ex}) with photoexcitation (E_{pump}) of 1.75 eV.

band-gap energy under all excitation-fluence conditions, indicating that the sample used in this study has no significant deep defect states, which are related to the radiative recombination process. Under weak excitation conditions (excitation fluence, $J_{ex} = 0.60 \mu\text{J}/\text{cm}^2$), an almost symmetric PL peak appears, with a peak energy that is slightly less than the E_{c1-v1} transition energy. As the excitation fluence increases to $J_{ex} = 36.6 \mu\text{J}/\text{cm}^2$, the peak energy of the PL spectrum reaches the E_{c1-v1} transition energy. This excitation-fluence-dependent peak shift is the result of the state filling due to the photocarriers. The E_{c1-v1} transition energy corresponds to the spatially averaged band-gap energy. Moreover, the relatively large peak shift of a few tens of millielectronvolts per decade strongly supports the existence of band-tail states, which are due to the potential fluctuation around the band edge.^{11,12,27,32,34}

Note that the PL spectra and dynamics reflect the dynamical behavior of the free and localized carriers. In cases involving complex semiconducting materials such as polycrystalline CIGS samples, in which the defects and grain boundaries affect the radiative recombination dynamics,^{19–25,27} it is difficult to determine the free electron and hole lifetimes accurately. Therefore, for an improved understanding of the free photocarrier dynamics in the CIGS thin films, we measured the TA dynamics at the two different optical transitions depicted in Fig. 1 and compared the results.

The TA signals versus both time and the photon energy of the CIGS thin films under a 1.24-eV excitation (the resonant excitation of the E_{c1-v1} transition) are plotted in Fig. 3(a). This excitation fluence was chosen in order to maintain low fluence within the linear-response regime, where many-body effects such as Auger recombination^{35,36} are negligible. Two broad positive ($\Delta T/T > 0$) signals can be observed at approximately 1.25 and 1.46 eV, which are attributed to photobleaching signals originating from the E_{c1-v1} and E_{c1-v3} transitions, respectively. The TA spectra at various delay times are also shown in Fig. 3(b). The two TA peaks appearing at approximately 1.25 and 1.46 eV correspond to the E_{c1-v1} and E_{c1-v3} transitions, respectively, and their energies show good agreement with the peak energies of Fig. 2(b). It is speculated that the oscillated fine structures in TA spectra at approximately 1.25 eV are likely caused by multiple

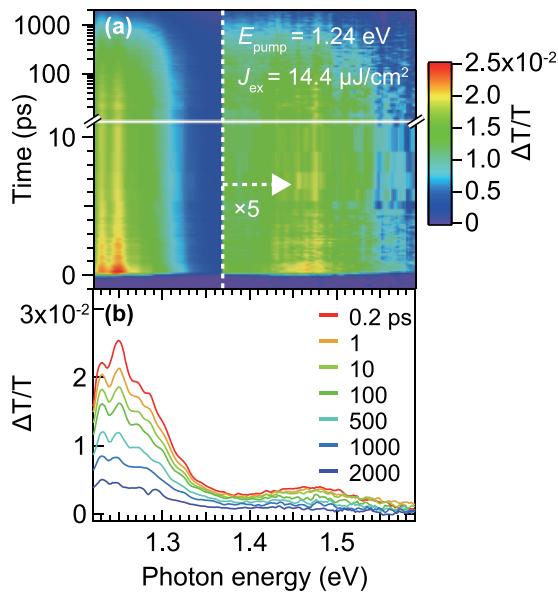


FIG. 3. (a) TA map of CIGS thin films under an excitation (E_{pump}) of 1.24 eV. (b) TA spectra of CIGS thin films for various delay times with photoexcitation of 1.24 eV.

reflection interference and scattering of probe pulses. As the delay time increases, both TA signals decrease monotonically but are still visible even at 2 ns. This clearly indicates that the photocarriers have long lifetimes, despite the existence of a large number of defects and grain boundaries in polycrystalline thin films.

Because a pump pulse with a photon energy of 1.24 eV (less than the E_{c1-v3} transition energy (~ 1.45 eV)) excites electrons from the $v1$ to the $c1$ bands, the TA signal intensity observed at approximately 1.46 eV reflects the electron population in the lowest conduction band ($c1$). On the other hand, the TA signal at approximately 1.25 eV reflects the dynamic behavior of both the electrons in the $c1$ band and the holes in the $v1$ band. This means that the comparison between the TA decay dynamics monitored for the E_{c1-v1} and E_{c1-v3} transitions allows us to distinguish between the conduction-band-electron and valence-band-hole dynamics. It is noteworthy that broadband TA measurement considering band structure is a key technique used to gain deeper insight into the photocarrier relaxation dynamics of complex systems.

To understand the relaxation dynamics of the conduction-band electrons and valence-band holes in CIGS thin films individually, we compared the excitation fluence dependence of the TA decay dynamics monitored at the E_{c1-v3} (~ 1.46 eV) transition with those obtained at the E_{c1-v1} (~ 1.23 eV) transition, as shown in Figs. 4(a) and 4(b), respectively. The pump energy was set to 1.24 eV so as to generate electrons in the lowest $c1$ band and holes in the highest $v1$ band. We can clearly observe that the TA decay dynamics differ from each other, especially under strong excitation-fluence conditions.

Here, we can evaluate the relaxation dynamics of the free electrons in the conduction band by analyzing the TA decay dynamics detected at 1.46 eV, since the TA decay dynamics of the E_{c1-v3} transition reflect only the free electron dynamics in the $c1$ band under the lowest-energy E_{c1-v1} resonant excitation, as mentioned previously. Under weak excitation-fluence conditions, the TA decay dynamics in

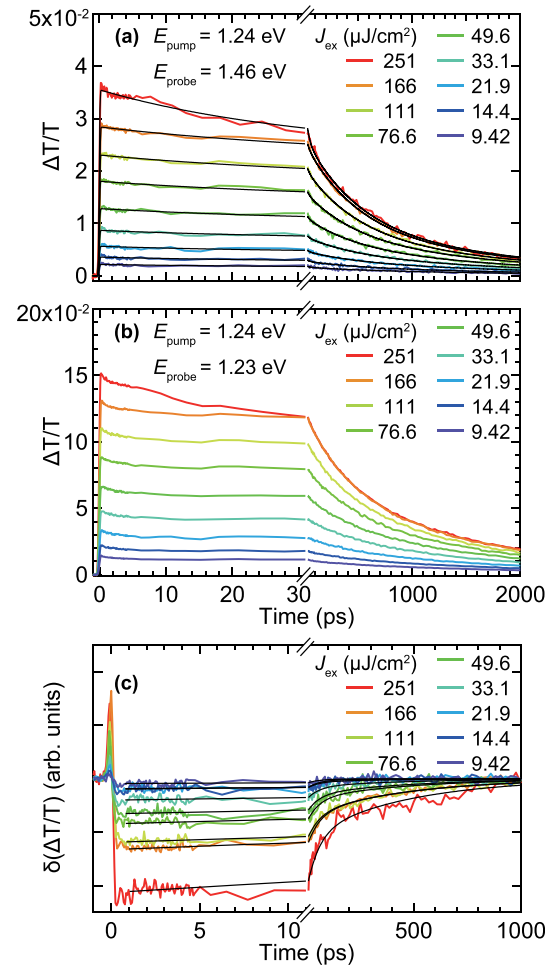


FIG. 4. Excitation fluence dependence of TA decay curves of CIGS thin films probed at $E_{\text{probe}} =$ (a) 1.46 eV and (b) 1.23 eV under photoexcitation (E_{pump}) of 1.24 eV. (c) Differential TA decay curves derived by subtracting the scaled TA decay dynamics monitored at 1.46 eV from those recorded at 1.23 eV for various excitation fluences. The black curves in (a) and (c) represent the fitted curves.

Fig. 4(a) are well represented by double exponential functions. The estimated decay time constants are ~ 20 – 30 ps and ~ 2 ns, respectively. An additional decay component of several hundreds of picoseconds appears and grows in intensity with increasing excitation fluence. Because the characteristic dependence of the dynamical behavior on the excitation fluence is quite similar to the previous results,²⁷ we attribute these decay components in ascending order of time constant to: (i) the electron trapping process in the donor states; (ii) the band-to-band transition; and (iii) the transition from the donor states to the $v1$ band.

To clarify the hole dynamics evident in the TA signal intensities observed at the E_{c1-v1} transition in Fig. 4(b), we subtracted the TA curves monitored at the E_{c1-v3} transition (the TA intensities due to the $c1$ -band electrons) from those obtained at the E_{c1-v1} transition (the TA intensities caused by the $c1$ -band electrons and the $v1$ -band holes) after normalization at long delay times of 1 ns. Here, we assumed that the long decay components of both TA curves were almost identical, because they are minimally affected by the relaxation processes related to the defect states and grain boundaries.²⁷ The differential TA decay curves are shown in Fig. 4(c). The large differential signals are negative, meaning that the

differential TA signals are primarily caused by the c1-band electrons. The sharp positive signals observed just after excitation originate from the difference in probe-pulse width, between 1.23 and 1.46 eV. Thus, we only discuss the differential TA decay dynamics after 1 ps. The negative differential TA curves in Fig. 4(c) are well fitted by double exponential functions and the obtained decay time constants are several tens and several hundreds of picoseconds in duration, which have almost the same order of magnitude as the electron-decay time constants. Thus, this finding also supports the observation that the differential TA decay curves primarily reflect the electron decay dynamics, and that the hole decay dynamics only minimally affect the TA signal decay at the E_{c1-v1} transition in the picosecond timescale up to 1 ns. Therefore, we conclude that the free holes have long lifetimes of greater than a few nanoseconds.

Finally, we briefly discuss the general features of the electron decay dynamics in the polycrystalline CIGS thin films through a comparison of two different types of CIGS sample. In this work, the TA decay component ratio of process (i) (the electron trapping process in the donor states) to process (iii) (the transition from the donor states to the v1 band) in the electron decay dynamics, corresponding to the trapping probability in the defect states, is one order of magnitude smaller than that of the previous study under weak excitation-fluence conditions.²⁷ In the former case, the sample was prepared through the 3-stage evaporation method, while, in the latter, the co-evaporation method, in which all elements are deposited simultaneously to form the CIGS layer, was used for sample preparation.²⁷ This result and the absence of PL emission far below the band gap indicate that the polycrystalline CIGS fabricated using the 3-stage process method has small deep-defect state density, which is related to the radiative recombination processes. Nevertheless, the TA decay dynamics of both samples show almost the same tendencies as regards the decay time constants and the evolution of the excitation fluence. This fact means that the dynamical behavior of the free electrons is minimally dependent on the defect state number and type, resulting in the robust and long lifetimes of the conduction-band electrons in polycrystalline CIGS. The existence of long-lived free electrons with lifetimes on a timescale of a few nanoseconds, despite the fast electron trapping, is one of the characteristic features of the highly efficient optoelectronic conversion exhibited by polycrystalline CIGS thin films. Our findings, therefore, provide a key information necessary for the design and optimization of high-efficiency CIGS-based solar cells.

In conclusion, we have revealed the photogenerated free-carrier dynamics in the lowest conduction and highest valence bands of CIGS thin films using white-light TA spectroscopy. Two clear photobleaching peaks were observed in the TA spectra, which originated from the optical transition from the highest and second-highest valence bands to the lowest conduction band. We can distinguish between the contributions of the electrons and holes to the TA decay dynamics and have clarified the relaxation dynamics of the electrons in the conduction band. It has been determined that the origin of the long decay component with a nanosecond-timescale in the TA decay dynamics can be attributed to both the long-lived free electrons and holes in the respective bands.

Part of this work was supported by The Sumitomo Electric Industries Group CSR Foundation and JST-CREST.

- ¹A. M. Gabor, J. R. Tuttle, D. S. Albin, M. A. Contreras, R. Noufi, and A. M. Hermann, *Appl. Phys. Lett.* **65**, 198 (1994).
- ²P. Jackson, D. Hariskos, E. Lotter, S. Paetel, R. Wuerz, R. Menner, W. Wischmann, and M. Powalla, *Prog. Photovoltaics* **19**, 894 (2011).
- ³S. Niki, M. Contreras, I. Repins, M. Powalla, K. Kushiya, S. Ishizuka, and K. Matsubara, *Prog. Photovoltaics* **18**, 453 (2010).
- ⁴B. Shin, O. Gunawan, Y. Zhu, N. A. Bojarczuk, S. J. Chey, and S. Guha, *Prog. Photovoltaics* **21**, 72 (2013).
- ⁵W. Wang, M. T. Winkler, O. Gunawan, T. Gokmen, T. K. Todorov, Y. Zhu, and D. B. Mitzi, *Adv. Energy Mater.* **4**, 1301465 (2014).
- ⁶H. Zhou, Q. Chen, G. Li, S. Luo, T.-B. Song, H.-S. Duan, Z. Hong, J. You, Y. Liu, and Y. Yang, *Science* **345**, 542 (2014).
- ⁷H. J. Snaith and M. Grätzel, *Adv. Mater.* **18**, 1910 (2006).
- ⁸J. E. Jaffe and A. Zunger, *Phys. Rev. B* **29**, 1882 (1984).
- ⁹S. B. Zhang, S.-H. Wei, A. Zunger, and H. Katayama-Yoshida, *Phys. Rev. B* **57**, 9642 (1998).
- ¹⁰S. Siebentritt, M. Igalson, C. Persson, and S. Lany, *Prog. Photovoltaics* **18**, 390 (2010).
- ¹¹I. Dirnstorfer, Mt. Wagner, D. M. Hofmann, M. D. Lampert, F. Karg, and B. K. Meyer, *Phys. Status Solidi A* **168**, 163 (1998).
- ¹²J. Krustok, H. Collan, M. Yakushev, and K. Hjelt, *Phys. Scr.* **T79**, 179 (1999).
- ¹³J. Kim, S. Kim, C.-S. Jiang, K. Ramanathan, and M. M. Al-Jassim, *Appl. Phys. Lett.* **104**, 063902 (2014).
- ¹⁴S. Lany and A. Zunger, *Phys. Rev. Lett.* **100**, 016401 (2008).
- ¹⁵J. Vidal, S. Botti, P. Olsson, J.-F. Guillemoles, and L. Reining, *Phys. Rev. Lett.* **104**, 056401 (2010).
- ¹⁶H. Mönig, Y. Smith, R. Caballero, C. A. Kaufmann, I. Lauermaun, M. Ch. Lux-Steiner, and S. Sadewasser, *Phys. Rev. Lett.* **105**, 116802 (2010).
- ¹⁷M. Hafemeister, S. Siebentritt, J. Albert, M. Ch. Lux-Steiner, and S. Sadewasser, *Phys. Rev. Lett.* **104**, 196602 (2010).
- ¹⁸S. S. Schmidt, D. Abou-Ras, S. Sadewasser, W. Yin, C. Feng, and Y. Yan, *Phys. Rev. Lett.* **109**, 095506 (2012).
- ¹⁹B. Ohnesorge, R. Weigand, G. Bacher, A. Forchel, W. Riedl, and F. H. Karg, *Appl. Phys. Lett.* **73**, 1224 (1998).
- ²⁰W. K. Metzger, I. L. Repins, and M. A. Contreras, *Appl. Phys. Lett.* **93**, 022110 (2008); W. K. Metzger, I. L. Repins, M. Romero, P. Dippo, M. Contreras, R. Noufi, and D. Levi, *Thin Solid Films* **517**, 2360 (2009).
- ²¹S. Shimakawa, K. Kitani, S. Hayashi, T. Satoh, Y. Hashimoto, Y. Takahashi, and T. Negami, *Phys. Status Solidi A* **203**, 2630 (2006).
- ²²T. Sakurai, K. Taguchi, M. M. Islam, S. Ishizuka, A. Yamada, K. Matsubara, S. Niki, and K. Akimoto, *Jpn. J. Appl. Phys., Part 1* **50**, 05FC01 (2011).
- ²³S. Shirakata, H. Ohta, and N. Iwado, *Jpn. J. Appl. Phys., Part 1* **51**, 10NC13 (2012).
- ²⁴O. Gunawan, T. K. Todorov, and D. B. Mitzi, *Appl. Phys. Lett.* **97**, 233506 (2010).
- ²⁵T. Gokmen, O. Gunawan, T. K. Todorov, and D. B. Mitzi, *Appl. Phys. Lett.* **103**, 103506 (2013).
- ²⁶S.-C. Chen, Y.-K. Liao, H.-J. Chen, C.-H. Chen, C.-H. Lai, Y.-L. Chueh, H.-C. Kuo, K.-H. Wu, J.-Y. Juang, S.-J. Cheng, T.-P. Hsieh, and T. Kobayashi, *Opt. Express* **20**, 12675 (2012).
- ²⁷M. Okano, Y. Takabayashi, T. Sakurai, K. Akimoto, H. Shibata, S. Niki, and Y. Kanemitsu, *Phys. Rev. B* **89**, 195203 (2014).
- ²⁸Y. Yamada, T. Nakamura, M. Endo, A. Wakamiya, and Y. Kanemitsu, *Appl. Phys. Express* **7**, 032302 (2014).
- ²⁹Y. Yamada, T. Nakamura, M. Endo, A. Wakamiya, and Y. Kanemitsu, *J. Am. Chem. Soc.* **136**, 11610 (2014).
- ³⁰L. Q. Phuong, M. Okano, Y. Yamada, A. Nagaoka, K. Yoshino, and Y. Kanemitsu, *Appl. Phys. Lett.* **104**, 081907 (2014).
- ³¹L. Q. Phuong, M. Okano, Y. Yamada, G. Yamashita, T. Morimoto, M. Nagai, M. Ashida, A. Nagaoka, K. Yoshino, and Y. Kanemitsu, *Appl. Phys. Lett.* **105**, 231902 (2014).
- ³²M. J. Romero, H. Du, G. Teeter, Y. Yan, and M. M. Al-Jassim, *Phys. Rev. B* **84**, 165324 (2011).
- ³³M. I. Alonso, M. Garriga, C. A. Durante Rincon, E. Hernandez, and M. Leon, *Appl. Phys. A* **74**, 659 (2002).
- ³⁴L. Q. Phuong, M. Okano, Y. Yamada, A. Nagaoka, K. Yoshino, and Y. Kanemitsu, *Appl. Phys. Lett.* **103**, 191902 (2013).
- ³⁵H. Yasuda and Y. Kanemitsu, *Phys. Rev. B* **77**, 193202 (2008).
- ³⁶Y. Kanemitsu, *Acc. Chem. Res.* **46**, 1358 (2013).